Complete anisotropic time-dependent heat equation in KTP crystal under repetitively pulsed Gaussian beams: a numerical approach

Mostafa Mohammad Rezaee, Mohammad Sabaeian,* Alireza Motazedian, Fatemeh Sedaghat Jalil-Abadi, and Ali Khaldi-Nasab

Department of Physics, Faculty of Science, Shahid Chamran University of Ahvaz, Ahvaz, Iran

*Corresponding author: sabaeian@scu.ac.ir

In this work, a thorough and detailed solution for the time-dependent heat equation for a cylindrical nonlinear potassium titanyl phosphate (KTP) crystal under a repetitively pulsed pumping source is developed. The convection and radiation boundary conditions, which are usually ignored in the literature, have been taken into account, and their importance on the temperature distribution has been discussed in detail. Moreover, the temperature dependence of thermal conductivity of KTP was considered in the calculations, and its impact is discussed. It is shown that the radiation term has a negligible effect and can be dropped safely, while the temperature dependence of thermal conductivity is more influential, such that ignorance of it brings some errors into the modeling. The time evolution of the temperature while the crystal is pumping with a train of successive Gaussian pulses until reaching equilibrium is shown. To accomplish numerical calculations, we developed a homemade code written with the finite difference time domain method in Intel Fortran (ifort) and ran it with the Linux operating system. © 2015 Optical Society of America

OCIS codes: (140.6810) Thermal effects; (190.0190) Nonlinear optics.
http://dx.doi.org/10.1364/AO.54.001241

1. Introduction

Nonlinear properties of media can be excited when they are exposed to intense laser beams. However, due to optical absorption, some of the irradiated energy converts to heat, where it can change the optical properties of the crystals leading to detrimental thermal effects. The thermal effect plays a critical role in solid-state and fiber lasers, since it may cause laser cavity instability [1], degradation of beam quality [2–6], crystal fracture and melting [7], and nonlinear effects [8,9]. Nonlinear changes in refractive index arise when the crystal is warmed up. The main contribution in refractive index changes, which is also known as thermal dispersion, is given by

$\Delta n = (\partial n / \partial T) \times \Delta T$ in which the temperature change depends on laser intensity. Accurate prediction of the amount of heat generated in the laser crystal is particularly of great importance in determining the size of the laser material and the pumping power to avoid strong thermal effects as well as to determine the cooling systems [7]. In practice, to reduce the thermal effect and prevent thermal damage to the crystal, cooling systems are mandatory; that means the crystal is covered by two layers of copper sheet, allowing cooling materials such as water or liquid nitrogen to flow between.

In the pumping schemes adopted for nonlinear crystals, the pump beam is irradiated along the crystal axis. Through the conduction cooling mechanism, heat is transferred to the outer boundaries, and it then is dissipated out by convection and radiation mechanisms. Therefore, the central parts of the

crystal and lateral side have the highest and lowest temperatures, respectively. Despite the fact that the crystal is cooled, due to the finite relaxation time of the thermal processes which depended on the crystal properties, the central parts would be always warmer, and so a temperature gradient occurs [10]. The thermal gradient causes thermal dispersion [11,12], thermally induced birefringence [13,14], end-face deformation or bulging [15], and thermal strains and stresses [8], where all of aforementioned phenomena lead to wavefront deformation [16,17].

Determining the temperature distribution in the solid-state media provides the possibility of studying the thermo-optical properties of different materials [18], wave-vector mismatching [19], analyzing the wavelength shift due to temperature rise in thin-film filters used for dense wavelength division multiplexing [20], measuring the weak absorption and defect identification of optical films [21], measuring the thermal conductivity of laser crystals [22], and thermal lens spectroscopy of various samples [23].

Numerous researches have been carried out to provide analytical solutions for the heat equation and obtaining the analytical formulas for the temperature distribution in solid-state laser crystals. However, without inserting simplifications in the heat equation, it is not possible to reach analytical solutions. Some simplifications which are usually made are as follow: ignoring the radiation and convection boundary conditions, ignoring the temperature dependency of thermal conductivity and thermal anisotropy of the crystal, and reducing some dimensions of the crystal. These simplifications can reduce the accuracy and applicability of analytical solutions, which are demonstrated in this work.

Sabaeian and Nadgaran [5] demonstrated that propagation of Bessel–Gauss beams can be severely influenced by generation of heat in the crystal. An analytical solution for steady state temperature distribution by taking only the r-dependent heat equation was reported by Schmid et al. [13]. A complicated solution for three-dimensional steady state heat equations for a cubic laser crystal with several simplifications in the boundary condition was presented by Li et al. [24]. A full analytical solution of the heat equation for an anisotropic Nd:YVO$_4$ crystal with cubic cross-section under a longitudinally Gaussian pump profile source was presented by Sabaeian et al. [10]. They took the pump power attenuation along the crystal and the real cooling mechanism of convection into account. Shi et al. [25] took the forward and backward pump absorption along the crystal axis into account, imposed the constant temperature and heat insulation conditions, and reported a semi-analytical expression for temperature distribution in the cylindrical coordinates for a Nd:YAG rod under diode end-pumping in a steady-state regime. Simultaneously, in another semi-analytical solution, Shi et al. considered a rectangular and anisotropic Nd:YVO$_4$ crystal and imposed the constant temperature condition for six sides [11]. Usievich et al. [26]

solved the time-dependent heat equation analytically in the cylindrical coordinates by making use of a Gaussian source and longitudinal absorption. Liu et al. [27] skillfully solved the heat equation in a double-clad fiber laser in the short transient regime. The repetitively pulsed pumping also has been taken into account, and analytical formulas have been derived for top-hat and time-profiled pulses. Transient temperature, thermal stress, and strain were calculated by Liu et al. They have found that the pulse shape has a noteworthy impact on thermal stress, and a reasonable design for the pulse duration and period can be utilized to reduce the thermal stress and optimize the performance of a high-power fiber laser. Bernhardi et al. [28] estimated the thermal fracture limits in quasi–continuous wave end-pumped lasers through a time-dependent analytical model. They reported the transient behavior of temperature and corresponding induced stresses on the pump face of an isotropic laser rod derived by making use of an analytical thermal model. Lausten and Balling [29] provided an analytical solution for the heat equation without a heat source for the short-transient regime. Their models, however, were useful only for a short pulsed pumping with top-hat and time-profiled pulses. Soon after that, Sabaeian and Nadgaran [23] developed a model for pulses with super-Gaussian profile. The influence of thermally induced phase mismatching in potassium titanyl phosphate (KTP) crystals for high-average power frequency doubling systems using a numerical model was investigated by Seidel and Mann [30]. They considered a spatial temperature distribution in a crystal anda correspondingwave-vector mismatching. They then derived an approximate analytical expression for the temperature profile from the heat-transfer equation in cylindrical symmetry. Sabaeian et al. [6] investigated the continuous wave second-harmonic generation and inspected the conversion efficiency of a KTP crystal under induced thermal load by coupling the heat equation with a second-harmonic generation (SHG) formalism applied to a type-II configuration. They demonstrated that in average and high power pumping, the thermal dephasing leads to a considerable reduction in SHG compared to ideal cases in which the induced heat is neglected. Recently, Sabaeian [31] proposed a general and an analytic solution for the anisotropic time-dependent heat equation for an arbitrary heat source in Cartesian coordinates with general Robin boundary conditions for a cubic-shaped solid state crystal. He applied his approach to investigate three different heat distributions: long transient, single-shot pumping or short transient, and repetitively pulsed pumping. He demonstrated the possibility of an easier and more accurate method to calculate the thermal dispersion, thermal stress/strain, thermal bending, and thermal phase shift. However, in this analysis, the temperature dependency of thermal conductivity as well as the cooling via radiation was neglected. With respect to the crucial influence

of thermal effect and a quickly developing technology in escalation of solid-state laser powers, there is a strong demand for a general solution for the heat equation with the least simplifications and approximations.

Therefore, in this work, we report a general solution for the anisotropic heat equation considering the most details, listed as follows: convection and radiation (which is a nonlinear condition) cooling mechanism, temperature dependence of thermal conductivity, and repetitively pulsed pumping heat source. To solve the heat equation with the aforementioned conditions, we adopted a homemade code written with the finite difference time domain (FDTD) method. In this regard, we have invented a new algorithm allowing us to reduce the run time and required temporary memory (RAM) to solve a time-dependent diffusion-type equation with repetitive pulse pumping in the cylindrical coordinates.

2. Heat Equation

The general form of the heat equation in an anisotropic solid-state material is given by [26]:

$$\rho c \frac{\partial T}{\partial t} + -\nabla.(K(T) \cdot \nabla T) = S, \tag{1}$$

where T is the temperature, ρ is the mass density, c is the specific heat, $K(T)$ is the temperature-dependent thermal conductivity, and S is the heat source. Through the use of Green's identity, Eq. (1) is rearranged as follows:

$$\rho c \frac{\partial T}{\partial t} - [\nabla.(K_r \nabla T|_r + K_\varphi \nabla T|_\varphi + K_z \nabla T|_z)] = S, \tag{2}$$

which, after imposing the divergence operator, leads to

$$\rho c \frac{\partial T}{\partial t} - \left[\frac{\partial K_r}{\partial r} \frac{\partial T}{\partial r} + K_r \frac{\partial^2 T_r}{\partial r^2} + \frac{\partial K_\varphi}{\partial \varphi} \frac{\partial T}{\partial \varphi} \right.$$
$$\left. + K_\varphi \frac{\partial^2 T_\varphi}{\partial \varphi^2} + \frac{\partial K_z}{\partial z} \frac{\partial T}{\partial z} + K_z \frac{\partial^2 T_z}{\partial z^2} \right] = S. \tag{3}$$

For the special case of an isotropic material, where $K_r(T) = K_\varphi(T) = K_z(T) = K(T)$, Eq. (3) is simplified to

$$\rho c \frac{\partial T}{\partial t} - \left(\left\{ \frac{\partial K(T)}{\partial r} \frac{\partial T}{\partial r} + \frac{\partial K(T)}{\partial \varphi} \frac{\partial T}{\partial \varphi} + \frac{\partial K(T)}{\partial z} \frac{\partial T}{\partial z} \right\} \right.$$
$$\left. + K(T) \{ \nabla_r^2 T + \nabla_\varphi^2 T + \nabla_z^2 T \} \right) = S. \tag{4}$$

In order to handle the anisotropic heat equation, Eq. (3), we need the tensor components of thermal conductivity. It is usually given in Cartesian coordinates rather than in cylindrical coordinates. Therefore, a transformation is needed to generate the components in the cylindrical coordinates. This transformation is given by

$$K_{r\varphi z}(T) = U^{-1} \cdot K_{xyz}(T).U(T), \tag{5}$$

where the dots mean tensor products, and U is given by

$$U = \begin{pmatrix} \cos \varphi & \sin \varphi & 0 \\ -\sin \varphi & \cos \varphi & 0 \\ 0 & 0 & 1 \end{pmatrix}, \tag{6}$$

where φ is the azimuth angle in cylindrical coordinates. Notice that the z component in both coordinate systems is the same.

As the Gaussian pump profile is symmetric azimuthally, the temperature is also symmetric azimuthally. Therefore, we can use

$$\frac{\partial K(T)}{\partial \varphi} = \nabla_\varphi^2 T = \frac{\partial T}{\partial \varphi} = 0, \tag{7}$$

and, therefore, we end up with the following equation for thermally anisotropic materials:

$$\rho c \frac{\partial T}{\partial t} - \left\{ \frac{\partial K_r}{\partial r} \frac{\partial T}{\partial r} + \frac{\partial K_z}{\partial z} \frac{\partial T}{\partial z} + K_r \frac{1}{r} \frac{\partial T}{\partial r} \right.$$
$$\left. + K_r \frac{\partial^2 T_r}{\partial r^2} + K_z \frac{\partial^2 T_z}{\partial z^2} \right\} = S. \tag{8}$$

The isotropic version of the heat equation is given by the following formula:

$$\rho c \frac{\partial T}{\partial t} - \left\{ \frac{\partial K}{\partial r} \frac{\partial T}{\partial r} + \frac{\partial K}{\partial z} \frac{\partial T}{\partial z} \right\} - K \left\{ \frac{1}{r} \frac{\partial T}{\partial r} + \frac{\partial^2 T}{\partial r^2} + \frac{\partial^2 T}{\partial z^2} \right\} = S. \tag{9}$$

With respect to this fact that KTP crystal shows a weak thermal anisotropic property, we continue our treatment by making a discretization on Eq. (9) using $T(t, r, z) \rightarrow T(i, j, k)$. So, the heat equation in discretized form will appeared as

$$T(i+1, j, k) = +T(i, j, k)$$
$$+ \frac{\Delta t}{\rho c} \frac{K(i, j+1, k) - K(i, j-1, k)}{2\Delta r} \frac{T(i, j+1, k) - T(i, j-1, k)}{2\Delta r}$$
$$+ \frac{\Delta t}{\rho c} \frac{K(i, j, k+1) - K(i, j, k-1)}{2\Delta z} \frac{T(i, j, k+1) - T(i, j, k-1)}{2\Delta z}$$
$$+ \frac{\Delta t}{\rho c} K(i, j, k) \frac{T(i, j+1, k) - T(i, j-1, k)}{2r\Delta r}$$
$$+ \frac{\Delta t}{\rho c} K(i, j, k) \frac{T(i, j+1, k) - 2T(i, j, k) + T(i, j-1, k)}{\Delta r^2}$$
$$+ \frac{\Delta t}{\rho c} K(i, j, k) \frac{T(i, j, k-1) - 2 \times T(i, j, k) + T(i, j, k+1)}{\Delta z^2}$$
$$+ \frac{\Delta t}{\rho c} S. \tag{10}$$

For $K(T)$, as a temperature-dependent thermal conductivity, we use an experimental formula which is given by [32–34]

$$K(T) = K_0 \times \frac{T_0}{T}. \qquad (11)$$

We use $T_0 = 300$ K, $K_0 = 13$ W (mK)$^{-1}$ [35], $\rho = 2945$ kgm^{-3}, and $c = 728.016$ J (kg · K)$^{-1}$.

For a pulsed pump with a Gaussian spatial–temporal profile, the heat source, S, is given by [31]

$$S = PQ_0 \exp[-2(r/\omega_f)^2] \exp(-\alpha z) \exp[-(t/t_p)^2], \quad (12)$$

where ω_f is the beam spot size, and α is the absorption coefficient of the crystal at laser (green) wavelength. Also,

$$P = \int_{-\infty}^{+\infty} E_0 \exp[-(t/t_p)^2]\mathrm{d}t = E_0/(t_p\pi^{1/2}) \qquad (13)$$

is the total power of the pulse with E_0 as the energy of the peak of the pulse. Q_0 is the normalization constant of the spatial part which is defined by [10]

$$Q_0 \int_0^{2\pi} \mathrm{d}\varphi \int_0^\infty e^{-2r^2/\omega_p^2} r\, \mathrm{d}r \int_0^L e^{-\alpha z}\mathrm{d}z = 1, \qquad (14)$$

leading to $Q_0 \simeq 2\alpha/\pi\omega_p^2$, where the assumption of $\exp(-\alpha L) \ll 1$ has been used [10,31].

The temperature of the boundaries must satisfy the following condition [10]:

$$-K(T)\hat{\mathbf{n}} \cdot \nabla T|_{\text{boundary}} = h(T_W - T_\infty) + \sigma\varepsilon(T_W^4 - T_s^4), \qquad (15)$$

where $\hat{\mathbf{n}}$ is an outward unit vector perpendicular to the surface. Equation (15) can be simplified to

$$-K(T)(\mp\hat{\mathbf{z}}) \cdot \left(\frac{\partial T}{\partial r}\hat{\mathbf{r}} + \frac{\partial T}{\partial \varphi}\hat{\varphi} + \frac{\partial T}{\partial z}\hat{\mathbf{z}}\right)\bigg|_{\text{boundary}}$$
$$= h(T_W - T_\infty) + \sigma\varepsilon(T_W^4 - T_s^4), \qquad (16)$$

where $-\hat{\mathbf{z}}$ and $+\hat{\mathbf{z}}$ belong to the beginning and end faces of the crystal, respectively. For cylindrical coordinates, we have $\hat{\mathbf{z}} \cdot \hat{\mathbf{r}} = \hat{\mathbf{z}} \cdot \hat{\varphi} = 0$. Therefore, the first and the second term on the right side of Eq. (16) will be suppressed. So it is reformed as

$$\pm \frac{\partial T}{\partial z}\bigg|_{\text{boundary}} = \frac{h(T_W - T_\infty) + \sigma\varepsilon(T_W^4 - T_s^4)}{K(T)}. \qquad (17)$$

$h = 10$ Wm^{-2} K^{-1} is the temperature convection coefficient [32]; $\sigma = 5.669 \times 10^{-8}$ Wm^{-2} K^{-4} is the Stephan–Boltzman constant; $\varepsilon = 0.9$ is the surface emission coefficient; and T_∞, T_W, and T_s are the temperature of the fluid moving around the surface, temperature of the surface (wall), and ambient temperature, respectively.

Figure 1(a) shows the geometry and the boundary conditions of investigated nonlinear crystal. The
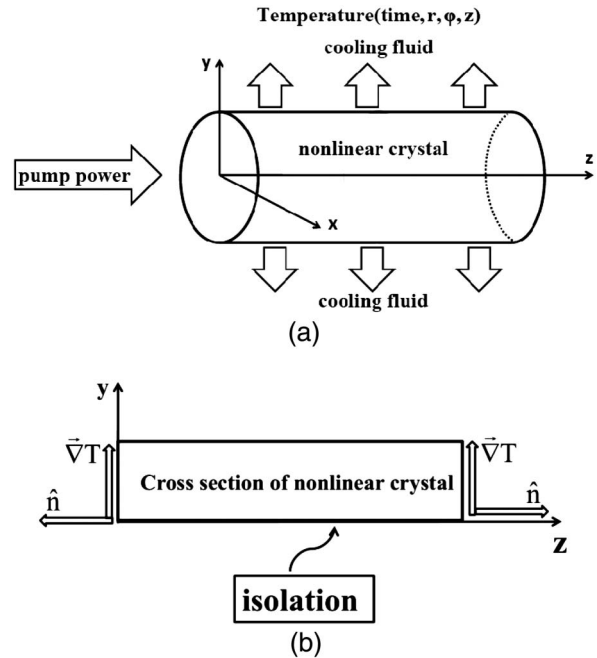

Fig. 1. (a) Geometry of KTP crystal with direction of pumping. For the lateral boundary the condition of constant temperature ($T = 300$ K) and for end faces the conditions of convection and radiation have been considered. (b) rz plane of KTP crystal. Due to azimuthal symmetry, we only take the rz plane of the crystals.

lateral surface is set to a constant temperature ($T = 300$ K). The convection and radiation boundary conditions are applied for input and output surfaces. According to azimuthal symmetry of the crystal, we took an rz plane, as depicted in Fig. 1(b). There is a temperature gradient from the $r = 0$ line to the lateral line ($r = a$) in the perpendicular direction. Therefore, the crystal axis with highest temperature acts as an insulation line, as the temperature cannot cross it. Consequently, the insulation boundary condition for the crystal axis ($r = 0$) is taken to provide the mathematical requirement of the problem.

3. Results and Discussion

In order to solve the heat equation and obtain the temperature, a homemade code with the FDTD method was developed in our group. We wrote this code in Intel Fortran (ifort) and ran it in a Linux operating system. As a case study, we have considered a cylindrical and nonlinear KTP crystal with the radius of $a = 5$ mm, length of $l = 2$ cm [30], absorption coefficient of $\alpha = 4$ m^{-1} [36,37], and thermal capacity of $c = 2945$ j(kgK)$^{-1}$ [35,37]. The energy of pulses has been taken to be $E = 0.09$ j (except for Fig. 7 in which $E = 0.45$ j has been used) with a time duration of $t_p = 50$ ms and a spot size of $\omega_f = 100$ mm. The pulse repetition frequency was set to $f = 500$ Hz.

A. Numerical Procedure

As mentioned earlier, in order to solve the heat equation, a numerical code was written. Without useful contrivances, it is not possible to reach a stable

and accurate solution in a logical run time. Furthermore, the accessible RAM in home-used computing machines is restricted. Therefore, the contrivances discussed below have been made.

First of all, Eq. (12) stands only for one pulse. To simulate a repetitively pulsed pumping case which is desirable in this work, we saved the temperature of the crystal at the last time step of each pulse as the initial temperature of the next pulse. By repeating this procedure, successive pulses are accounted for and a repetitively pulsed pumping scheme is simulated. Overall, the temperature depends on five parameters: number of pulses, number of time steps, and three numbers that stand for radial, azimuthal, and longitudinal coordinates' steps. By dropping the azimuth coordinate, because of symmetry in the pumping profile, our primary estimation showed that the appropriate array lengths at which the solution converges should be $N_p = 1000$ (for number of pulses), $N_t = 4000$ (for number of time steps), $N_r = 500$ (for number of radial steps), and $N_z = 58$ (for number of axial steps). Therefore, the temperature should be a four-dimensional array with 1.16×10^{11} members. If it is supposed that for each member of such an array only one byte is needed, which is a quite underestimated rough number, we need 116GB of RAM, which is not practically possible. So, in the next step to reduce the members of the temperature array, we omitted the index of number of pulses in our code. We changed the code to store only the data of the last pulse, which is itself quite arbitrary and depends on how many pulses are going to be reported. Therefore, we did not allow the code to keep all pulses' data in RAM. This scheme reduced the number of array members by a factor of 4000 (the number of pulses). However, the number of array members is still large and out of the capability of our computing systems. The next step to reduce the array's members is discarding all time step data except that of ith time step which is used for the $(i + 1)$th time step [see Eq. (10)]. With this idea, only the data of two successive time steps, namely i and $i + 1$, are kept in the RAM. Therefore, we reduced further the number of temperature array members to 58×10^3, which is quite logical for home-used computing machines. In conclusion, we reduced the required RAM volume by a factor of 5×10^9. With this idea, the run time for a microsecond pulse which, was already several hours, is reduced to only 5 s.

B. Numerical Results

Figure 2(a) shows the time evolution of the temperature after irradiation with two successive pulses. As is seen, the temperature rise is much quicker than its lowering. More important is an accumulative behavior of temperature. Since the cooling process is prolonged, between two successive pulses when no energy is irradiated, the temperature drops. The rate of temperature rise depends on the thermal properties of the crystal, that is, thermal diffusivity, which is defined as $D = K/(\rho c)$. With respect to Eq. (12),
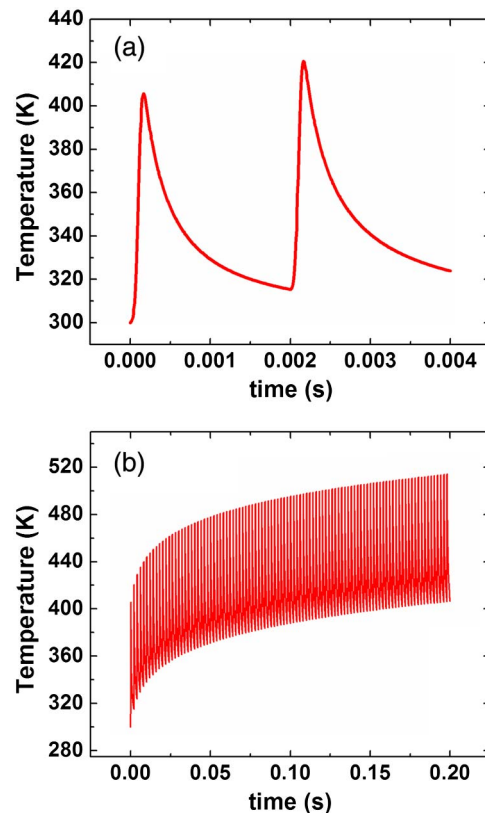

Fig. 2. Temporal variations of temperature at $r = 0$ and $z = 0$ for (a) 2 pulses and (b) 100 pulses.

where the heat source just simulates only one single pulse as $\exp(-t^2/t_p^2)$, in order to simulate the repetitively pulsed pumping, we used the following idea: the final temperature of the first pulse just before irradiating the second one, at any point of the crystal, was considered as an initial temperature for the next pulse. The procedure has been continued for the next pulses. This trace of such an idea can be seen clearly in Fig. 2(a). Figure 2(b) illustrates the case for repetitively pulsed pumping. With increasing the number of pulses, the temperature goes toward its steady state. Pronounced fluctuations are seen in the temperature, forming during the off-time between two successive pulses. At steady state, the peaks of pulses are equal in value.

Figure 3(a) represents the spatial distribution of the temperature along the r axis, and Fig. 3(b) shows it along the z axis, both for 1, 2, 10, 100, and 5000 pulses. Figure 3(a) shows that with increasing the number of pulses, the temperature tails back toward the crystal lateral surface; that is, its half width at half maximum increases. For longitudinal variations, with increasing the number of pulses, the temperature shows a steeper slope from the beginning to the end face of the crystal. This happens because the heat energy accumulates gradually at the beginning face of the crystal, and cooling mechanisms are no longer robust enough to dissipate it.

It is safe to say that when the repetition rate of irradiating pulses is increased, the overall
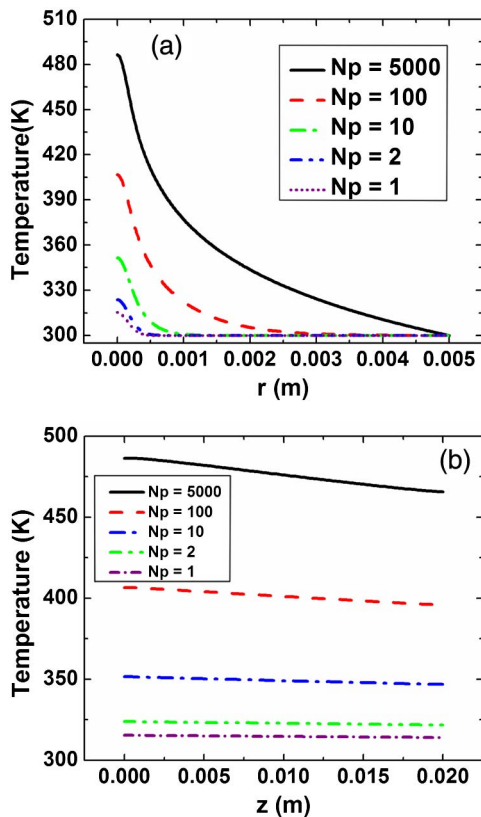
Fig. 3. Temperature distribution for different numbers of pulses (a) in the radial direction of the input face and (b) along the crystal axis.
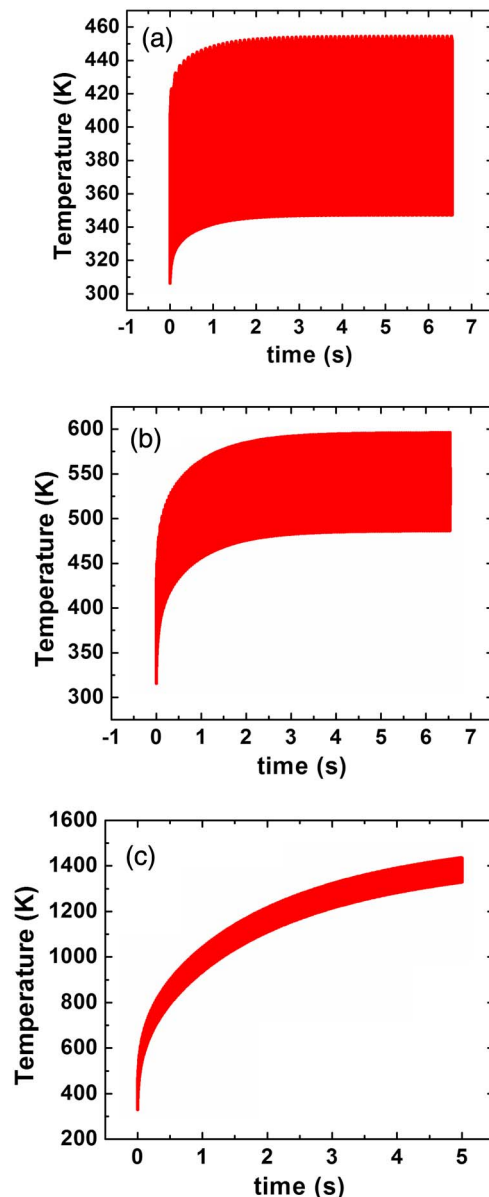

Fig. 4. Temporal variations of temperature for 1000 pulses irradiated to the crystal for repetition frequencies of (a) 200, (b) 500, and (c) 1000 Hz.

temperature of the crystal increases. This happens due to lowering the time-off between successive pulses. Figures 4(a), 4(b), and 4(c) compare three different frequencies of 200, 500, and 1000 Hz, respectively. It is clear to see that with increasing the repetition frequency, the fluctuations in temperature lower and the overall temperature increases.

Having found the temperature distribution and its variations in time, one can simply calculate the thermal conductivity as a function of position and time in the crystal through the expression $K[T(\mathbf{r}, t)] = K_0 \times T_0/T(\mathbf{r}, t)$. Figure 5(a) reports that when the temperature increases as time collapses, the thermal conductivity reduces noticeably. The lowering of thermal conductivity leads to reduction in heat dissipation, so that the crystal temperature is enhanced compared to the ideal case in which the thermal conductivity is taken to be constant. As Fig. 5(a) shows, the steady-state thermal conductivity is around $5 \, \mathrm{Wm^{-1} \, K^{-1}}$, while its value at $T = 300 \, \mathrm{K}$ is $13 \, \mathrm{Wm^{-1} \, K^{-1}}$. Figure 5(b) shows the spatial variations of thermal conductivity along the radial direction. As the figure shows, thermal conductivity takes larger values at the crystal boundary ($r \sim a$), as a result of lowering the temperature at that place. The longitudinal variations of thermal conductivity are plotted in Fig. 5(c). The figure clearly shows the difference between the constant and temperature-dependent thermal conductivity. Furthermore,

recalling the fact that the temperature is lower at the end parts of the crystal than the beginning parts, the thermal conductivity is somehow larger.

Figure 6(a) compares the crystal's temperature of the ideal case (constant thermal conductivity) with the realistic case (temperature-dependent thermal conductivity) as a function of time. The figure shows a lower temperature when a temperature-dependent thermal conductivity is used. Also, along the radial [Fig. 6(b)] and longitudinal directions [Fig. 6(c)], the temperature-dependent case shows noticeable higher values for temperature.

In order to complete our discussion, we consider various boundary conditions to see which ones are more important and play a crucial role in determining the temperature and which ones are less
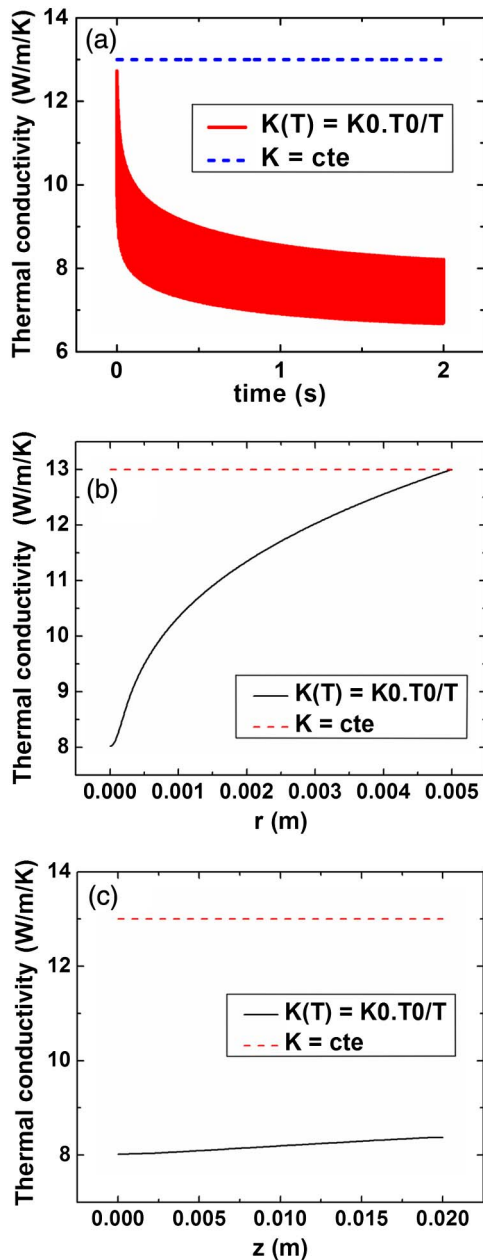
Fig. 5. Variations of thermal conductivity (a) as a function of time for the center of the input face, (b) along the radial direction of the input face, and (c) along the crystal axis.
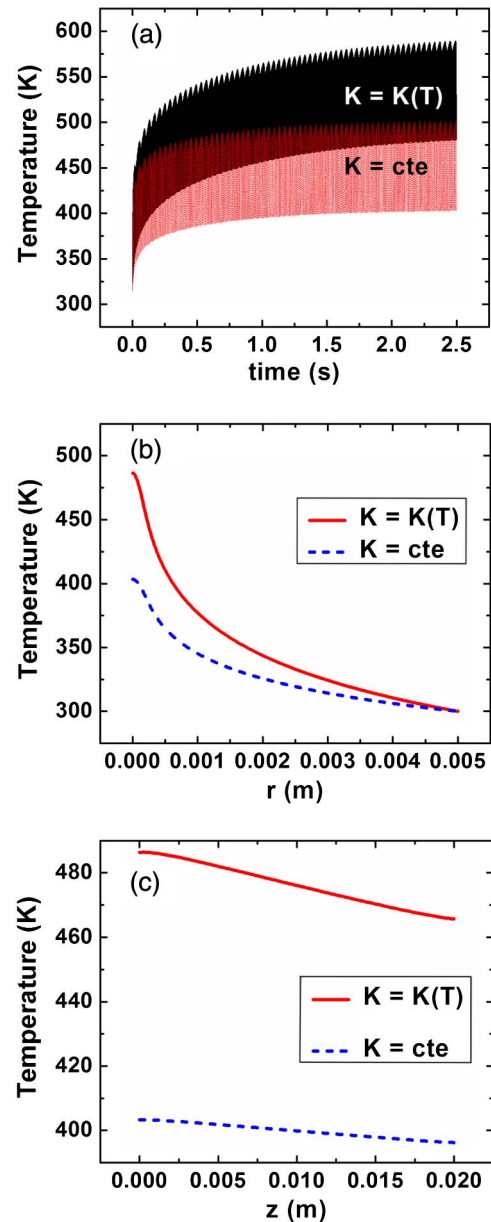

Fig. 6. Temperature variations (a) as a function of time for the center of the input face, (b) along the radial direction of the input face, and (c) along the crystal axis. The blue curves (solid) show the constant thermal conductivity, and the red curve (dashed) shows the temperature-dependent case.

important and can be safely discarded. We note that so far, all of the results have been obtained for a beam spot size of $\omega_f = 100$ μm. Nevertheless, we found that to reveal the difference between various boundary conditions, bigger spot sizes should be applied. So $\omega_f = 1500$ μm is used in the following. In Figs. 7(a)–7(c), we set the lateral surface temperature to $T = 300$ K, as before, but used various boundary conditions for the beginning and end faces of the crystal. Figure 7(a) shows the temporal variations of temperature at $r = 0$ and $z = 0$ for the isolation condition (dotted–dotted–dashed and black curve), convection condition only (dashed and green curve), radiation condition only (dotted and blue curve), and

both radiation and convection conditions together (solid and red curve). Figures 7(b) and 7(c) show the same results but along the radial and longitudinal directions, respectively. The results all emphasize that the radiation affects the temperature only at the regions near the beginning and end faces of the crystal. In the middle points and in the regions near the crystal circumference, radiation has no noticeable impact. Convection in the presence of radiation does not show a noticeable impact, so it can be safely discarded. The isolation of two faces of the crystal, which is not proposed in such systems, gives a higher temperature at the crystal faces, although it gives the same temperature as the radiation only
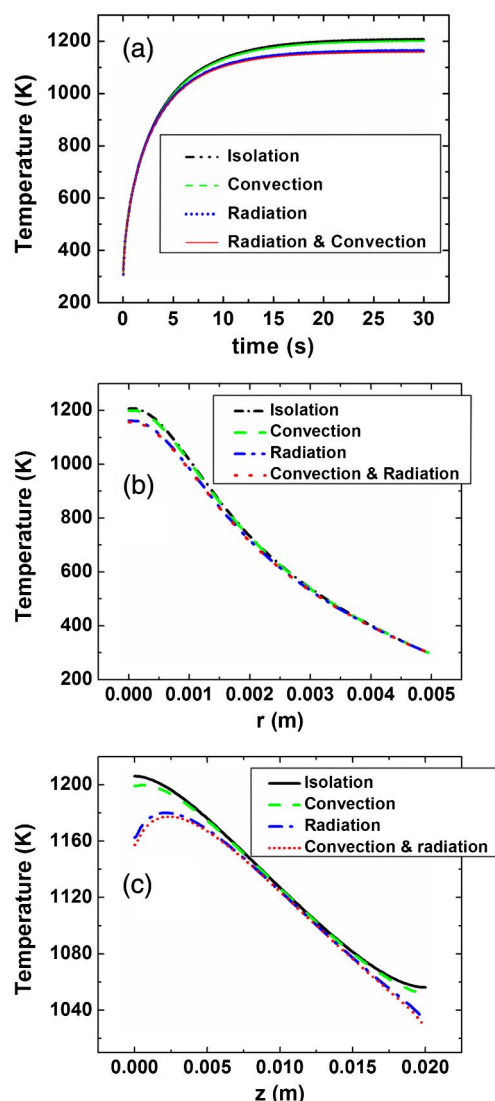
Fig. 7. (a) Temporal variations of the temperature at the input face, (b) the temperature along the radial direction at the input face, and (c) the temperature along the axial direction. The boundary conditions are isolation (black), convection (green), radiation (blue), and convection and radiation together (red).

and the radiation with convection at the points far from the crystal faces.

4. Conclusion

In this work, the heat equation for a cylindrical KTP crystal under a repetitively pulsed pumping scheme has been solved numerically. A numerical code has been developed with the FDTD method. The temperature dependence of thermal conductivity as well as the various temperature boundary conditions have been considered, and their impact on the temperature distribution has been examined. The results confirmed an inevitable effect for temperature dependence of thermal conductivity on the temperature of the crystal. Although it is not possible, to the best of our knowledge, to present an analytical solution when temperature-dependent thermal conductivity is taken into account, its role in the solution is much more important. Also, it was shown that the thermal insulation and convection condition gives a higher temperature for the beginning and end faces of the crystal compared to the case in which radiation is used. We concluded that the heat radiation from crystal faces and its contribution in cooling dominates other cooling mechanisms, indicating that it should be considered if an accurate value for temperature is desirable. An interesting point is that, for middle parts of the crystal, all temperature conditions give the same values. Therefore, one can simply drop all complicated temperature boundary conditions if the temperature of the crystal's face is not desirable. The reason is that the area of the lateral surface at which the heat is removed via perfect convection ($h \rightarrow \infty$) is dominantly larger than those of end faces at which radiation or convection (with low coefficient) occurs. For crystals with large end face areas, the results of this work must be used with care.

References

1. X. Jiang, X. Yuan, H. Yu, M. Xu, D. Cao, and W. Duan, "Influence of the thermal effect on stability of the output in a heat capacity laser," Chin. Opt. Lett. **5**, S19–S20 (2007).
2. I. Mukhin, O. Palashov, E. Khazanov, A. Ikesue, and Y. Aung, "Experimental study of thermally induced depolarization in Nd:YAG ceramics," Opt. Express **13**, 5983–5987 (2005).
3. H. Nadgaran and M. Servatkhah, "The effects of induced heat loads on the propagation of Ince–Gaussian beams," Opt. Commun. **284**, 5329–5337 (2011).
4. H. Nadgaran, M. Servatkhah, and M. Sabaeian, "Mathieu–Gauss beams: a thermal consideration," Opt. Commun. **283**, 417–426 (2010).
5. M. Sabaeian and H. Nadgaran, "Bessel–Gauss beams: investigations of thermal effects on their generation," Opt. Commun. **281**, 672–678 (2008).
6. M. Sabaeian, L. Mousave, and H. Nadgaran, "Investigation of thermally-induced phase mismatching in continuous-wave second harmonic generation: a theoretical model," Opt. Express **18**, 18732–18743 (2010).
7. D. C. Brown, "Heat, fluorescence, and stimulated-emission power densities and fractions in Nd:YAG," IEEE J. Quantum Electron. **34**, 560–572 (1998).
8. D. C. Brown and H. J. Hoffman, "Thermal, stress, and thermo-optic effects in high average power double-clad silica fiber lasers," IEEE J. Quantum Electron. **37**, 207–217 (2001).
9. M. Sabaeian, F. S. Jalil-Abadi, M. M. Rezaee, and A. Motazedian, "Heat coupled Gaussian continuous-wave double-pass type-II second harmonic generation: inclusion of thermally induced phase mismatching and thermal lensing," Opt. Express **22**, 25615–25628 (2014).
10. M. Sabaeian, H. Nadgaran, and L. Mousave, "Analytical solution of the heat equation in a longitudinally pumped cubic solid-state laser," Appl. Opt. **47**, 2317–2325 (2008).
11. P. Shi, W. Chen, L. Li, and A. Gan, "Semianalytical thermal analysis on a Nd:YVO$_4$ crystal," Appl. Opt. **46**, 4046–4051 (2007).
12. M. Sabaeian and H. Nadgaran, "Investigation of thermal dispersion and thermally-induced birefringence on high-power double clad Yb:glass fiber laser," Int. J. Opt. Photon. **2**, 25–31 (2009).
13. M. Schmid, T. Graf, and H. Weber, "Analytical model of the temperature distribution and the thermally induced birefringence in laser rods with cylindrically symmetric heating," J. Opt. Soc. Am. B **17**, 1398–1404 (2000).

14. L. Mousavi, M. Sabaeian, and H. Nadgaran, "Thermally-induced birefringence in solid-core photonic crystal fiber lasers," Opt. Commun. **300**, 69–76 (2013).
15. Z. Xiong, Z. G. Li, N. Moore, W. Huang, and G. Lim, "Detailed investigation of thermal effects in longitudinally diode-pumped Nd:YVO$_4$ lasers," IEEE J. Quantum Electron. **39**, 979–986 (2003).
16. J.-C. Chanteloup, F. Druon, M. Nantel, A. Maksimchuk, and G. Mourou, "Single-shot wave-front measurements of high-intensity ultrashort laser pulses with a three-wave interferometer," Opt. Lett. **23**, 621–623 (1998).
17. B. Schäfer, J. Gloger, U. Leinhos, and K. Mann, "Photo-thermal measurement of absorptance losses, temperature induced wavefront deformation and compaction in DUV-optics," Opt. Express **17**, 23025–23036 (2009).
18. F. Jürgensen and W. Schröer, "Studies on the diffraction image of a thermal lens," Appl. Opt. **34**, 41–50 (1995).
19. N. Barnes, R. Eckhardt, D. Gettemy, and L. Edgett, "Absorption coefficients and the temperature variation of the refractive index difference of nonlinear optical crystals," IEEE J. Quantum Electron. **15**, 1074–1076 (1979).
20. S. L. Prins, A. C. Barron, W. C. Herrmann, and J. R. McNeil, "Effect of stress on performance of dense wavelength division multiplexing filters: thermal properties," Appl. Opt. **43**, 633–637 (2004).
21. S.-H. Li, H.-B. He, Y.-G. Shan, D.-W. Li, Y.-A. Zhao, and Z.-X. Fan, "Enhanced surface thermal lensing for absorption evaluation and defect identification of optical films," Appl. Opt. **49**, 2417–2421 (2010).
22. M. Shimosegawa, T. Omatsu, T. Tateda, I. Ogura, J. L. Blows, P. Wang, and J. M. Dawes, "Thermal conductivity of a self-frequency-doubling laser crystal measured by use of optical methods," Appl. Opt. **40**, 1372–1377 (2001).
23. M. Sabaeian and H. Nadgaran, "An analytical model for finite radius dual-beam mode-mismatched thermal lens spectroscopy," J. Appl. Phys. **114**, 133102 (2013).
24. Z. Li, X. Huai, Y. Tao, and Z. Guo, "Analysis of thermal effects in an orthotropic laser medium," Appl. Opt. **48**, 598–608 (2009).
25. P. Shi, W. Chen, L. Li, and A. Gan, "Semianalytical thermal analysis of thermal focal length on Nd:YAG rods," Appl. Opt. **46**, 6655–6661 (2007).
26. B. A. Usievich, V. A. Sychugov, F. Pigeon, and A. Tishchenko, "Analytical treatment of the thermal problem in axially pumped solid-state lasers," IEEE J. Quantum Electron. **37**, 1210–1214 (2001).
27. T. Liu, Z. Yang, and S. Xu, "Analytical investigation on transient thermal effects in pulse end-pumped short-length fiber laser," Opt. Express **17**, 12875–12890 (2009).
28. E. Bernhardi, A. Forbes, C. Bollig, and M. Esser, "Estimation of thermal fracture limits in quasi–continuous-wave end-pumped lasers through a time-dependent analytical model," Opt. Express **16**, 11115–11123 (2008).
29. R. Lausten and P. Balling, "Thermal lensing in pulsed laser amplifiers: an analytical model," J. Opt. Soc. Am. B **20**, 1479–1485 (2003).
30. S. Seidel and G. Mann, "Numerical modeling of thermal effects in nonlinear crystals for high-average-power second harmonic generation," in *Photonics West '97* (International Society for Optics and Photonics, 1997), pp. 204–214.
31. M. Sabaeian, "Analytical solutions for anisotropic time-dependent heat equations with Robin boundary condition for cubic-shaped solid-state laser crystals," Appl. Opt. **51**, 7150–7159 (2012).
32. C. Pfistner, R. Weber, H. Weber, S. Merazzi, and R. Gruber, "Thermal beam distortions in end-pumped Nd:YAG, Nd:GSGG, and Nd:YLF rods," IEEE J. Quantum Electron. **30**, 1605–1615 (1994).
33. H. Glur, R. Lavi, and T. Graf, "Reduction of thermally induced lenses in Nd:YAG with low temperatures," IEEE J. Quantum Electron. **40**, 499–504 (2004).
34. C. Ong, E. Sin, and H. Tan, "Heat-flow calculation of pulsed excimer ultraviolet laser's melting of amorphous and crystalline silicon surfaces," J. Opt. Soc. Am. B **3**, 812–814 (1986).
35. J. D. Bierlein and H. Vanherzeele, "Potassium titanyl phosphate: properties and new applications," J. Opt. Soc. Am. B **6**, 622–633 (1989).
36. P. Perkins and T. Fahlen, "20-W average-power KTP intracavity-doubled Nd:YAG laser," J. Opt. Soc. Am. B **4**, 1066–1071 (1987).
37. D. Nikogosian, *Nonlinear Optical Crystals: A Complete Survey* (Springer, 2005).